

# Beyond the odd number limitation: a bifurcation analysis of time-delayed feedback control

W. Just

*School of Mathematical Sciences, Queen Mary,  
University of London, Mile End Road, London E1 4NS, UK\**

B. Fiedler and M. Georgi

*Institut für Mathematik, FU Berlin, Arnimallee 2-6, D-14195 Berlin, Germany*

V. Flunkert, P. Hövel, and E. Schöll

*Institut für Theoretische Physik, Technische Universität  
Berlin, Hardenbergstraße 36, 10623 Berlin, Germany*

(Dated: June 24, 2007)

## Abstract

We investigate the normal form of a subcritical Hopf bifurcation subjected to time-delayed feedback control. Bifurcation diagrams which cover time dependent states as well are obtained by analytical means. The computations show that unstable limit cycles with an odd number of positive Floquet exponents can be stabilised by time-delayed feedback control, contrary to incorrect claims in the literature. The model system constitutes one of the few examples where a nonlinear time delay system can be treated entirely by analytical means.

PACS numbers: 05.45.Gg,02.30.Ks,02.30.Oz

Keywords: control of chaos, time-delay dynamics, bifurcation analysis

---

\*Electronic address: [w.just@qmul.ac.uk](mailto:w.just@qmul.ac.uk)

## I. INTRODUCTION

Time-delayed feedback schemes are a simple but efficient tool to control unstable time-periodic target states in nonlinear dynamical systems [1]. Such methods have proven their experimental relevance in quite diverse contexts (cf., e.g., [2] and references therein). Various forms of the feedback control including multiple delay times [3] and applications to spatially extended systems, e.g. [4–7], have been considered. However, a deeper theoretical analysis of the control scheme was hampered for quite a while since time delay causes the corresponding phase space to become infinite-dimensional [8, 9]. At least from the point of view of linear stability analysis there is nowadays quite a substantial analytical knowledge about time-delayed feedback schemes available [10, 11]. In that context it has been claimed that time-delayed feedback schemes suffer from the so called odd-number limitation [12], i.e., unstable periodic orbits with an odd number of unstable positive Floquet multipliers cannot be stabilised by time-delayed feedback control. This claim has been refuted recently [13]. Actually, the results in [13] have been based on a simple model system, a normal form for a subcritical Hopf bifurcation, which can be solved essentially in analytical terms even when the time-delayed feedback control force has been applied. Thus, such a model is one of the few time delay systems that allow for deeper analytical insight beyond the linear regime. It thus fills the gap between abstract theoretical results about time delay dynamics and numerical simulations of time-delayed feedback control.

Such kind of mathematical models are quite common in nonlinear dynamics as they capture generic features of real physical systems. Actually, their origin dates back at least one century when van der Pol investigated the properties of nonlinear electronic circuits [14]. Nowadays, these approaches are used in such diverse contexts like laser dynamics [15], hydrodynamics and pattern formation [16], or bioscience [17]. Whenever the dynamical system undergoes an instability and develops an oscillating state the essential features of the motion can be captured, by virtue of an appropriate coordinate transformation, by a complex valued coordinate and the corresponding equation of motion reduces to a normal form [18]. Here, we present a fairly complete bifurcation analysis of such a kind of model. The model will be introduced in section II and the main results are briefly described in terms of bifurcation diagrams. The main control mechanism consists in the occurrence of transcritical bifurcations when the control amplitude is increased. Sections III-V are

devoted to the analytical computation of the different elements in the bifurcation diagrams. Further consequences for the control performance will be pointed out as well. To keep the presentation self-contained some standard analytical tools are summarised in appendices A and B. A brief summary from a mathematical viewpoint is contained in appendix C which puts the analysis in a broader context.

## II. MODEL SYSTEM AND BIFURCATION DIAGRAMS

As a generic model system for time-delayed feedback control of periodic orbits we consider the normal form of the subcritical Hopf bifurcation. In terms of the complex valued coordinate  $z(t)$  the equation of motion with time-delayed feedback control reads [13]

$$\dot{z}(t) = (\lambda + i)z(t) + (1 + i\gamma)|z(t)|^2z(t) - K \exp(i\beta)(z(t) - z(t - \tau)) \quad (1)$$

where  $\lambda$  and  $\gamma$  are real parameters,  $\lambda$  determines the distance from the Hopf bifurcation point of the uncontrolled system, and the Hopf frequency is normalised to unity. The parameter  $\gamma$  governs the dependence of the oscillation frequency on the amplitude, an effect which is often called detuning in the context of nonlinear oscillators. Actually, such a feature turns out to be quite important in the mathematical context of twist maps and plays a prominent role for pattern formation as well when nonlinear dispersion relations become relevant. Thus, it is not surprising that the parameter  $\gamma$  will become an important quantity for our investigations as well. Finally, control is governed by the real valued control amplitude  $K$  and a phase  $\beta$  which will turn out to be a crucial quantity in our context. The delay time is denoted by  $\tau \geq 0$ . The system without control,  $K = 0$ , has a stable or unstable trivial fixed point  $z_* = 0$  for  $\lambda < 0$  or  $\lambda > 0$ , respectively. For simplicity let us assume throughout our analysis that  $\gamma\lambda < 1$  holds. An unstable periodic orbit  $z(t) = R_P \exp(i\Omega_P t)$  with minimal period and amplitude

$$T_P = \frac{2\pi}{\Omega_P} = \frac{2\pi}{1 - \gamma\lambda} \quad (2a)$$

$$R_P = \sqrt{-\lambda} \quad (2b)$$

then exists for  $\lambda < 0$ . This particular orbit is the target state which we want to stabilise by time-delayed feedback control. A *noninvasive control scheme* requires the delay  $\tau$  to be an integer multiple of the minimal period  $T_P$ , and we will mainly concentrate here on the

simplest choice

$$\tau = T_P, \quad (\lambda < 0) \quad . \quad (3)$$

For some parts of the analysis it turns out to be useful to rewrite Eq. (1) in terms of real valued coordinates  $x_1 + ix_2 = z$

$$\begin{aligned} \begin{pmatrix} \dot{x}_1(t) \\ \dot{x}_2(t) \end{pmatrix} &= \begin{pmatrix} \lambda & -1 \\ 1 & \lambda \end{pmatrix} \begin{pmatrix} x_1(t) \\ x_2(t) \end{pmatrix} + (x_1^2(t) + x_2^2(t)) \begin{pmatrix} 1 & -\gamma \\ \gamma & 1 \end{pmatrix} \begin{pmatrix} x_1(t) \\ x_2(t) \end{pmatrix} \\ &\quad - K \begin{pmatrix} \cos \beta & -\sin \beta \\ \sin \beta & \cos \beta \end{pmatrix} \begin{pmatrix} x_1(t) - x_1(t - \tau) \\ x_2(t) - x_2(t - \tau) \end{pmatrix} \quad . \end{aligned} \quad (4)$$

Since the linear part of the model without control commutes with the control matrix, the dynamics still shares the nice properties of diagonal control schemes as far as analytic linear stability analysis is concerned. The two-dimensional representation (4) is equivalent to the complex representation (1).

The model, Eq. (1) or (4), has five parameters,  $\lambda$ ,  $K$ ,  $\tau$ ,  $\beta$ , and  $\gamma$ . The phase angle  $\beta$  may be confined to an interval of length  $\pi$  if the control amplitude  $K$  is allowed to take both positive and negative values. Throughout our numerical diagrams we will usually fix the two parameters  $\gamma = -10$  and  $\beta = \pi/4$  and we will consider two-dimensional cross sections in the remaining three-dimensional parameter space, although our analysis will cover more general cases as well. Since we will not impose the constraint (3) on the delay from the very beginning, we gain additional insight into the structure of the dynamics. Specifically, Eq. (3) determines a surface in the three-dimensional parameter space which we call *Pyragas manifold*.

Results are summarised in bifurcation diagrams. The corresponding analytical calculations will be presented in the subsequent sections. If we fix the control amplitudes below a certain threshold value  $K_c$ , then Fig. 1 shows the typical structure of the bifurcation diagram. It contains a wavy Hopf bifurcation line with alternating sub- (solid red) and supercritical (dashed green) behaviour. The trivial fixed point  $z_* = 0$  is stable to the left of the Hopf bifurcation line and unstable on the other side. If the Hopf bifurcation is subcritical, an unstable periodic orbit is generated on the left hand side of the line, whereas in the supercritical case a stable limit cycle bifurcates to the right of the line. Furthermore, the diagram contains saddle-node bifurcation lines (dotted black) which indicate a generation or annihilation of a pair of limit cycles. Such lines terminate at those points on the

Hopf bifurcation line which mark the transition between sub- and supercritical behaviour. If one takes into account that the system without delay  $\tau = 0$  has no limit cycle for  $\lambda > 0$ , then one can easily reconstruct the number of small limit cycles which occur in each part of the bifurcation diagram. The curve of parameter values which obey the condition (3), i.e., where the minimal period  $T_P$  of the unstable orbit (2) matches the delay  $\tau$ , is indicated as well (solid blue and dashed cyan). If the control amplitude is below the threshold value  $K_c$ , this *Pyragas curve* appears left of the Hopf bifurcation line. For such parameter values the periodic solution (2), namely the periodic orbit of the system without control, is also a solution of the time delay system. Close to the Hopf bifurcation line this particular periodic solution has at least one positive Floquet eigenvalue. But for smaller values of  $\lambda$  this eigenvalue becomes negative, i.e., a transcritical bifurcation occurs, and two periodic solutions interchange their stability. This bifurcation point can be clearly identified as a tangency between the Pyragas curve and a saddle-node bifurcation line.

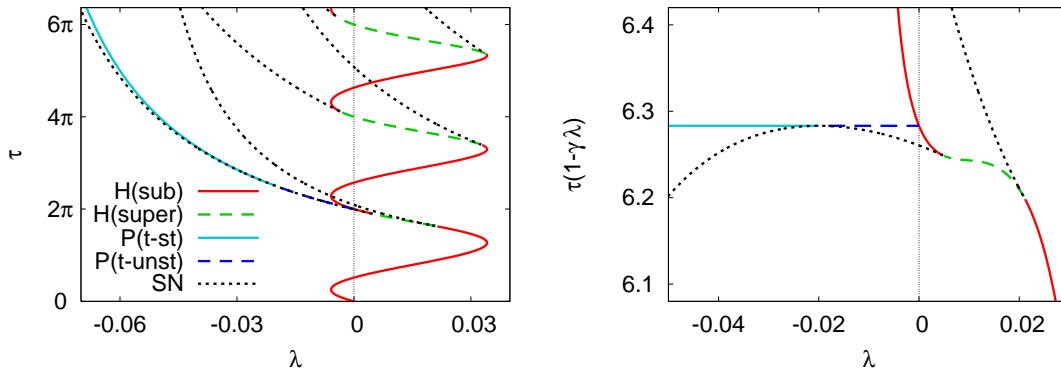


FIG. 1: (Color online) Left: Two-dimensional bifurcation diagram of Eq. (1) for  $\gamma = -10$ ,  $\beta = \pi/4$ , and  $K = 0.02$ : subcritical Hopf bifurcation (solid red/dark), supercritical Hopf bifurcation (dashed green/light), saddle-node (SN) bifurcation of limit cycles (dotted black), transcritical stable Pyragas curve (solid cyan/light), and transcritical unstable Pyragas curve (dashed blue/dark). Right: the same diagram enlarged close to  $\lambda = 0$ ,  $\tau = 2\pi$ , and displayed in distorted coordinates so that the Pyragas curve is a straight line.

If one increases the control amplitude, the transcritical bifurcation point moves along the Pyragas curve towards the Hopf bifurcation line and merges at a critical value with a transition from sub- to supercritical behaviour. When increasing the control amplitude beyond this critical value the Pyragas curve occurs right of the Hopf bifurcation line. The

latter has now turned to be supercritical. The transcritical bifurcation has disappeared and the saddle-node bifurcation has detached from the Pyragas curve (cf. Fig. 2). In particular, the periodic orbit on the Pyragas curve is now stable, at least close to the Hopf bifurcation, according to common wisdom about supercritical bifurcations.

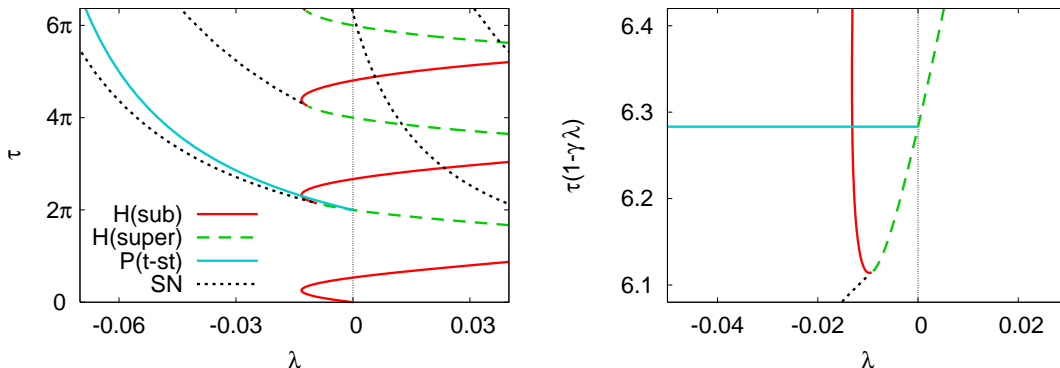


FIG. 2: (Color online) Left: two-dimensional bifurcation diagram of Eq. (1) for  $\gamma = -10$ ,  $\beta = \pi/4$ , and  $K = 0.045$ : subcritical Hopf bifurcation (solid red/dark), supercritical Hopf bifurcation (dashed green/light), saddle-node (SN) bifurcation of limit cycles (dotted black), and transcritical stable Pyragas curve (solid cyan/light). Right: the same diagram enlarged close to  $\lambda = 0$ ,  $\tau = 2\pi$ , displayed in distorted coordinates so that the Pyragas curve is a straight line.

Thus, the two bifurcation diagrams contain the main mechanism by which control of the unstable periodic orbit (2) is achieved. The model (1) has the nice property that all the details can be computed by analytical means. The explicit formulae are supplied in the following sections. Furthermore, we will dwell on a presentation of the data which is better suited to spot the control performance.

### III. BIFURCATION OF THE TRIVIAL SOLUTION

Stability of the trivial fixed point  $z_* = 0$  is evaluated straightforwardly by calculating the complex eigenvalue  $\Lambda$  from the characteristic equation of the linearised Eq. (1)

$$\Lambda = \lambda + i - K \exp(i\beta)(1 - \exp(-\Lambda\tau)) \quad . \quad (5)$$

Note that in the real valued representation (4) the eigenvalues appear as complex conjugate pairs. A Hopf bifurcation of the trivial state occurs for  $\Lambda = i\Omega_H$ , which gives the condition

$$i\phi/\tau = \lambda + i - K \exp(i\beta)(1 - \exp(-i\phi)) \quad (6)$$

where  $\phi = \Omega_H\tau$  denotes the rescaled critical frequency. Splitting Eq. (6) into real and imaginary parts yields the Hopf curve in the  $(\lambda, \tau)$  parameter plane, or a surface in the  $(\lambda, \tau, K)$  parameter space, with parametric representation

$$\lambda = K(\cos\beta - \cos(\beta - \phi)) \quad (7a)$$

$$\tau = \frac{\phi}{1 - K(\sin\beta - \sin(\beta - \phi))} \quad (7b)$$

which is equivalent to the explicit form  $\tau_H(\lambda)$  derived in [13]. The behaviour of the bifurcation curve becomes quite intricate for large values of  $\tau$  but here we mainly focus on values of the delay in a neighbourhood of the Pyragas manifold, i.e., values of order  $\mathcal{O}(1)$ . By construction the Hopf bifurcation is subcritical for  $K = 0$ , i.e., in the singular limit  $\tau = 0$ . Thus subcritical behaviour prevails for small values of  $K$  and  $\tau$ . To uncover the nature of the Hopf bifurcation for general parameter values a normal form reduction of Eq. (4) can be performed (cf. appendix A for details). Super- and subcritical behaviour is then distinguished by the sign of the coefficient of the cubic nonlinearity and yields the criterion

$$1 + K\tau(\cos(\beta - \phi) + \gamma \sin(\beta - \phi)) \begin{cases} < 0 & \text{supercritical} \\ > 0 & \text{subcritical} \end{cases} \quad (8)$$

where the control amplitude  $K$  and the delay time  $\tau$  are determined by Eqs. (7). Eqs. (7) with condition (8) define the sub- and supercritical Hopf curves displayed in Figs. 1 and 2. A codimension-two bifurcation, i.e., a transition from sub- to supercritical behaviour, occurs when the expression given in Eq. (8) vanishes.

#### IV. STABILITY PROPERTIES ON THE PYRAGAS MANIFOLD

Let us now consider values for the delay which coincide with the period of the target state, i.e., let us constrain the analysis to the Pyragas manifold which is determined by the condition (2a) and (3)

$$\tau = \tau_P(\lambda) = \frac{2\pi}{1 - \gamma\lambda}, \quad \lambda < 0 \quad (9)$$

By construction the nonlinear equation (1) admits the periodic orbit (2) as a solution for all parameter values on this manifold. The boundary of this manifold, i.e., its endpoint in the two-dimensional  $(\lambda, \tau)$  parameter plane, is given by  $(\lambda, \tau) = (0, 2\pi)$ . Thus the Pyragas manifold terminates at the Hopf bifurcation line since the endpoint satisfies Eqs. (7) with the particular choice  $\phi = 2\pi$ . We first concentrate on the orientation of the Pyragas manifold with respect to the Hopf bifurcation line by computing the gradient of both curves at  $(\lambda, \tau) = (0, 2\pi)$ . Eq. (9) yields for the slope of the Pyragas curve

$$\left. \frac{d\tau_P}{d\lambda} \right|_{\lambda=0} = 2\pi\gamma \quad (10)$$

while the slope of the Hopf bifurcation line  $\tau_H(\lambda)$  at the same point is evaluated implicitly from Eqs. (7) to be

$$\left. \frac{d\tau_H}{d\lambda} \right|_{\lambda=0} = -\frac{2\pi}{\tan \beta} - \frac{1}{K \sin \beta} \quad (11)$$

Both gradients coincide at the critical point

$$K_c = -\frac{1}{2\pi(\cos \beta + \gamma \sin \beta)}, \quad \tau_c = 2\pi, \quad \lambda_c = 0 \quad (12)$$

If  $K \sin \beta < K_c \sin \beta$ , that means  $K < K_c$  if we confine the phase  $\beta$  to the interval  $[0, \pi]$ , then the Hopf bifurcation line is steeper than the Pyragas curve and the latter is locally to the left of the Hopf bifurcation line. For control parameter values larger than the critical value the orientation of both lines is interchanged, i.e., the periodic orbit (2) appears to the right of the Hopf bifurcation line (cf. Figs. 1 and 2). Furthermore, such a geometry implies that at that stage the Hopf bifurcation has become supercritical. In fact, the codimension three point (12) necessarily obeys the analytical conditions for the codimension-two Hopf bifurcation with degenerate cubic coefficient (cf. Eqs. (7) and (8) with  $\phi = 2\pi$ ). Such arguments have already been used in [13] to determine the regime of stabilisation of the Pyragas orbit in the complex plane of the control parameter  $Ke^{i\beta}$ .

In order to complete this picture let us investigate the stability of the periodic orbit (2) on the Pyragas manifold (9). Using the ansatz  $z(t) = R_P \exp(i\Omega_P t)(1 + \delta r(t) + i\delta\varphi(t))$  and expanding the equation of motion (1) to linear order in the small deviations  $\delta r, \delta\varphi$  around



the periodic orbit we obtain

$$\begin{aligned} \begin{pmatrix} \dot{\delta r}(t) \\ \dot{\delta\varphi}(t) \end{pmatrix} &= \begin{pmatrix} -2\lambda & 0 \\ -2\lambda\gamma & 0 \end{pmatrix} \begin{pmatrix} \delta r(t) \\ \delta\varphi(t) \end{pmatrix} \\ &\quad - K \begin{pmatrix} \cos\beta & -\sin\beta \\ \sin\beta & \cos\beta \end{pmatrix} \begin{pmatrix} \delta r(t) - \delta r(t - \tau) \\ \delta\varphi(t) - \delta\varphi(t - \tau) \end{pmatrix} . \end{aligned} \quad (13)$$

Since in the amplitude and phase variables  $\delta r, \delta\varphi$  the Jacobian matrix does not depend on time, the Floquet exponents of the periodic orbit are simply given by the eigenvalues  $\Lambda$  of the characteristic equation

$$\begin{aligned} 0 &= [2\lambda + \Lambda + K \cos\beta(1 - \exp(-\Lambda\tau))] [\Lambda + K \cos\beta(1 - \exp(-\Lambda\tau))] \\ &\quad + [2\lambda\gamma + K \sin\beta(1 - \exp(-\Lambda\tau))] K \sin\beta(1 - \exp(-\Lambda\tau)) \\ &= [\Lambda + K \exp(i\beta)(1 - \exp(-\Lambda\tau))] [\Lambda + K \exp(-i\beta)(1 - \exp(-\Lambda\tau))] \\ &\quad + 2\lambda [\Lambda + (\cos\beta + \gamma \sin\beta)K(1 - \exp(-\Lambda\tau))] . \end{aligned} \quad (14)$$

Obviously the characteristic equation admits the solution  $\Lambda = 0$  which corresponds to the Goldstone mode of the limit cycle, i.e. the trivial Floquet mode with Floquet multiplier one. Let us first study stability changes caused by real eigenvalues. Expansion of Eq. (14) up to second order yields

$$\begin{aligned} 0 &= 2\lambda\Lambda (1 + (\cos\beta + \gamma \sin\beta)K\tau) \\ &\quad + \Lambda^2 (|1 + K\tau \exp(i\beta)|^2 - \lambda\tau K\tau(\cos\beta + \gamma \sin\beta)) + \mathcal{O}(\Lambda^3) . \end{aligned} \quad (15)$$

A second nontrivial vanishing eigenvalue occurs if the linear part vanishes, i.e.

$$K\tau = -\frac{1}{\cos\beta + \gamma \sin\beta} . \quad (16)$$

Such a condition marks the occurrence of a transcritical bifurcation since the Goldstone mode supplies the necessary symmetry to the system. If we consider, for instance, cases such that the coefficient of the second order term in the expansion (15) is positive, i.e.,  $|1 + K\tau \exp(i\beta)|^2 + \lambda\tau > 0$ , then the condition for stability and instability with respect to this transcritical mode is easily written down

$$1 + (\cos\beta + \gamma \sin\beta)K\tau \begin{cases} < 0 & \text{transcritical stable} \\ > 0 & \text{transcritical unstable} \end{cases} . \quad (17)$$

Such a criterion is, of course, only a necessary condition since on the one hand it does not take into account complex conjugate eigenvalues, and on the other hand it holds only in a neighbourhood of the transcritical point. But a closer inspection reveals that the condition for a transcritical unstable mode is actually a sufficient criterion for an unstable periodic orbit. The right hand side of the characteristic equation (14) grows quadratically when considered for real values of  $\Lambda$ , while a transcritical unstable mode tells us that its gradient is negative at  $\Lambda = 0$ . Thus, there is at least one real positive solution in such a case. We therefore apply Eq. (17) as a global criterion along the Pyragas curve, keeping in mind that stability may require additional conditions caused by complex solutions of the characteristic equation.

If the parameters approach the critical point (12) then the transcritical point tends towards the critical point as well since the constraint (12) obeys Eq. (16). Thus, at the critical point the transcritical bifurcation on the Pyragas manifold and the transition from sub- to supercritical on the Hopf bifurcation line merge and both manifolds, the Pyragas and the Hopf line, exchange their mutual orientation (cf. Figs. 1 and 2).

To evaluate the stability of the periodic orbit (2) on the Pyragas manifold one has to address all complex valued solutions of Eq. (14). There is apparently no simple way to develop necessary and sufficient conditions. A brief discussion is given in appendix B which actually shows that for values of  $\lambda$  close to zero large parts of the transcritical stable branch are actually stable. But if  $|\lambda|$  exceeds a certain threshold value stabilisation cannot be achieved any longer. Such a feature seems to be quite common among time-delayed feedback schemes [19] since strongly unstable orbits are notoriously difficult to tackle by such control schemes.

## V. DELAY-INDUCED PERIODIC ORBITS

In the previous section we have analysed the Pyragas orbit of the delay system, which is also an unstable periodic orbit of the system without control  $K = 0$ . Of course, the delay may induce other periodic orbits as well, and the analysis of such states will elucidate the mechanism of the transcritical bifurcation. General bifurcation theory already predicts that a saddle-node bifurcation line of limit cycles starts at each codimension-two Hopf bifurcation point. Furthermore, a saddle-node bifurcation line of limit cycles touches the Pyragas

manifold at the transcritical bifurcation point. Thus, the investigation of delay-induced periodic orbits yields additional essential details of the bifurcations which trigger control of the Pyragas orbit (2).

Computing general periodic solutions of Eq. (1) is of course a difficult problem. Here we focus on harmonic solutions (rotating waves)  $z(t) = R \exp(i\Omega t)$  which can be computed straightforwardly by analytical means thanks to the rotational symmetry of the system. Eq. (1) yields

$$R^2 = -\lambda + K(\cos \beta - \cos(\beta - \varphi)) \geq 0 \quad (18a)$$

$$\varphi = \tau(1 - \lambda\gamma) + K\tau(\gamma \cos \beta - \sin \beta - \gamma \cos(\beta - \varphi) + \sin(\beta - \varphi)) \quad (18b)$$

where  $\varphi = \Omega\tau$  abbreviates the normalised frequency of the orbit. Condition (18) determines harmonic orbits which occur in pairs, since the equation results in the intersection between a harmonic function and the diagonal (cf. Fig. 3).

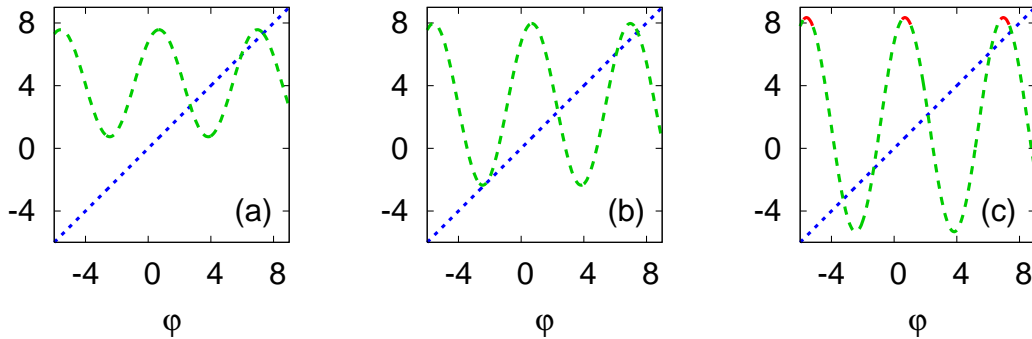


FIG. 3: (Color online) Graphical solution of the condition (18b) for  $\gamma = -10$ ,  $\beta = \pi/4$ ,  $\lambda = -0.02$ ,  $\tau = 8$ , and different values of the control amplitude: (a)  $K = 0.04$ , (b)  $K = 0.0604$ , (c)  $K = 0.08$ . Dotted blue: left-hand side of Eq. (18b), dashed green/solid red: right-hand side of Eq. (18b) such that the inequality (18a) is valid/invalid. (cf. Fig. 6)

Whenever the diagonal touches the graph generated by the right hand side of Eq. (18b), a saddle-node bifurcation takes place, provided that the inequality (18a) is satisfied. Thus, the condition for a saddle-node bifurcation of limit cycles reads

$$K\tau = -\frac{1}{\gamma \sin(\beta - \varphi) + \cos(\beta - \varphi)} \quad (19a)$$

$$\tau(1 - \lambda\gamma) = \varphi - K\tau(\gamma \cos \beta - \sin \beta - \gamma \cos(\beta - \varphi) + \sin(\beta - \varphi)) \quad (19b)$$

$$\lambda \leq K(\cos(\beta) - \cos(\beta - \varphi)) \quad . \quad (19c)$$

The constraint (19c) ensures that the saddle-node bifurcation line terminates at the sub-supercritical Hopf transition since the corresponding parameters (cf. Eqs. (7) and (8)) satisfy Eqs. (19) with  $\varphi = \phi$  and equality in Eq. (19c). Furthermore, a saddle-node line passes through the transcritical point since the corresponding conditions, Eqs. (9) and (16), are fulfilled by Eqs. (19) with the choice  $\varphi = 2\pi$ . The bifurcation diagram shows these features as well (cf. Fig. 1). If the control amplitude passes through the codimension three point (12), the saddle-node line detaches from the Pyragas manifold (cf. Fig. 2). Furthermore, on changing the control amplitude sub-supercritical Hopf transitions may collide. In such cases the corresponding two saddle-node bifurcation lines merge, detach from the Hopf line, and a cusp point is generated (cf. Fig. 4).

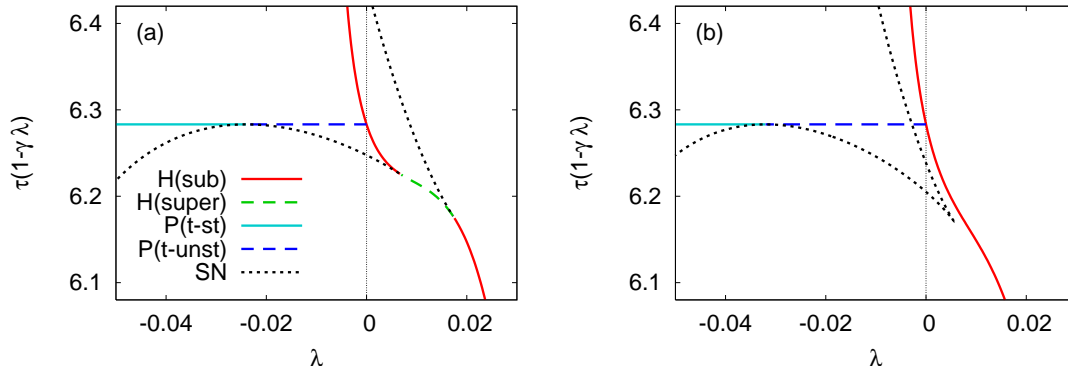


FIG. 4: (Color online) Bifurcation diagram of Eq. (1) for  $\gamma = -10$ ,  $\beta = \pi/4$  in distorted coordinates (cf. Fig. 1) for different values of the control amplitude, (a)  $K = 0.019$ , (b)  $K = 0.016$ . Subcritical Hopf bifurcation (solid red/dark), supercritical Hopf bifurcation (dashed green/light), saddle-node (SN) bifurcation of limit cycles (dotted black), transcritical stable Pyragas curve (solid cyan/light), and transcritical unstable Pyragas curve (dashed blue/dark).

Alternatively, we may think of Fig. 4 as a projection of a higher-dimensional bifurcation diagram, including the phase space coordinates as well, onto the two-dimensional parameter plane  $(\lambda, \tau(1 - \lambda\gamma))$ . If we plot instead of the infinite-dimensional phase space just a single component, e.g., the radius of the periodic orbit, then Fig. 5 shows how pairs of periodic orbits coalesce and disappear as we decrease  $\tau$  through the saddle-node curve. Along this fold surface of periodic orbits the tangent Pyragas curve distinguishes two curves of periodic orbits which intersect the saddle-node curve transversely, and mutually transversely, at what appears as a tangency in the parameter projection of Fig. 4. In particular, the bifurcation

of periodic orbits is transcritical when restricted to the Pyragas curve.

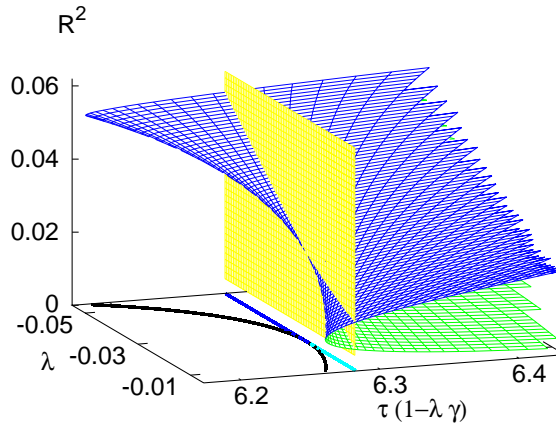


FIG. 5: (Color online) Unfolding of the transcritical bifurcation for  $\gamma = -10$ ,  $\beta = \pi/4$  and  $K = 0.019$  (cf. Fig. 4a). Blue/green surface: parameter dependence of the periodic orbits according to Eq. (18). Yellow surface: orthogonal projection of the Pyragas orbit onto the parameter plane. Black line: saddle-node bifurcation line as a projection of the fold. Blue/cyan line: Pyragas line as a projection of the unstable/stable Pyragas orbit onto the parameter plane.

So far we have considered bifurcation diagrams as two-dimensional slices in a  $(\lambda, \tau)$  parameter plane. From the control perspective it seems, however, more appropriate to focus on other cross sections, e.g., a  $(K, \tau)$  control parameter plane for fixed values of  $\lambda$ . Such diagrams are of course easily produced using Eqs. (7) and (8) for the Hopf bifurcation line of the trivial fixed point, Eqs. (9) and (17) for the properties of the Pyragas curve, and Eqs. (19) for the saddle-node bifurcation lines of rotating waves. Figure 6 contains data for  $\lambda = -0.02$ . The Pyragas orbit (2) becomes stable through a transcritical bifurcation when increasing the control amplitude  $K$  and it stays stable throughout the displayed range of control amplitudes as the analysis in appendix B shows (cf. Fig. 9). Furthermore, quite a large number of delay-induced limit cycles is generated for large values of the control amplitude (cf. also Eq. (19b) and Fig. 3).

Finally, one may have a closer look at the transcritical bifurcation and at the periodic orbits that are involved in the exchange of stability. The amplitude of the rotating wave in dependence on, say, the control amplitude is easily evaluated from Eq. (18). If we confine the analysis to the Pyragas manifold, i.e., if we consider delays which obey the constraint

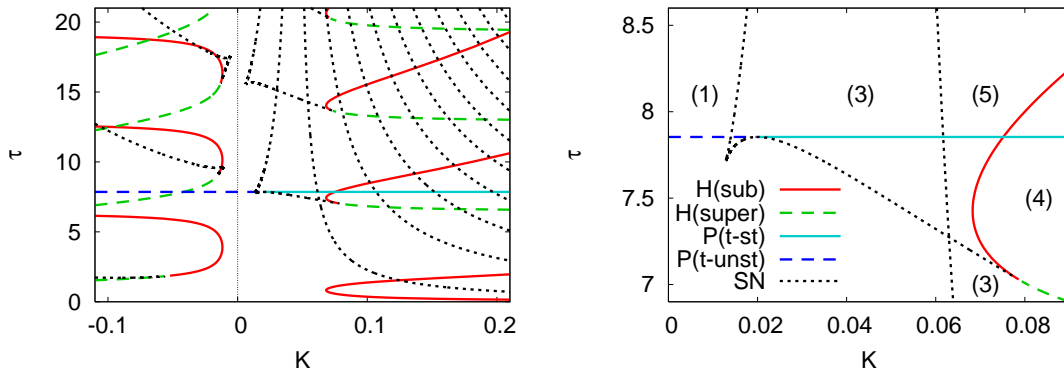


FIG. 6: (Color online) Left: two-dimensional bifurcation diagram of Eq. (1) for  $\gamma = -10$ ,  $\beta = \pi/4$ , and  $\lambda = -0.02$  in the control parameter plane: subcritical Hopf bifurcation (solid red/dark), supercritical Hopf bifurcation (dashed green/light), saddle-node (SN) bifurcation of limit cycles (dotted black), transcritical stable Pyragas curve (solid cyan/light), and transcritical unstable Pyragas curve (dashed blue/dark). Right: enlarged section. Labels indicate the number of harmonic solutions of the system.

(9) and consider the same parameter values used in Fig. 6 we obtain the diagram displayed in Fig. 7. Clearly this slice shows that the transcritical bifurcation is caused by the stable limit cycle generated in the saddle-node bifurcation. The remaining unstable periodic orbit disappears at larger values of the control amplitude in the subcritical Hopf bifurcation of the trivial fixed point. It is expected, and can be shown by arguments involving two-dimensional centre manifolds, that this unstable periodic orbit generates the basin boundary between the still stable trivial solution and the stabilised Pyragas orbit (cf. [20]). Furthermore, if we decrease the control amplitude adiabatically and cross the control threshold one still will observe a periodic motion but with a non-vanishing control signal and with a period which now changes with the control amplitude, i.e., one observes the stable delay-induced periodic orbit.

## VI. CONCLUSION

We have analytically studied the bifurcations in a nonlinear model system subjected to time-delayed feedback control. Such a model can be viewed as a paradigm for nonlinear time delay dynamics near a subcritical Hopf bifurcation. It has recently been used [13]

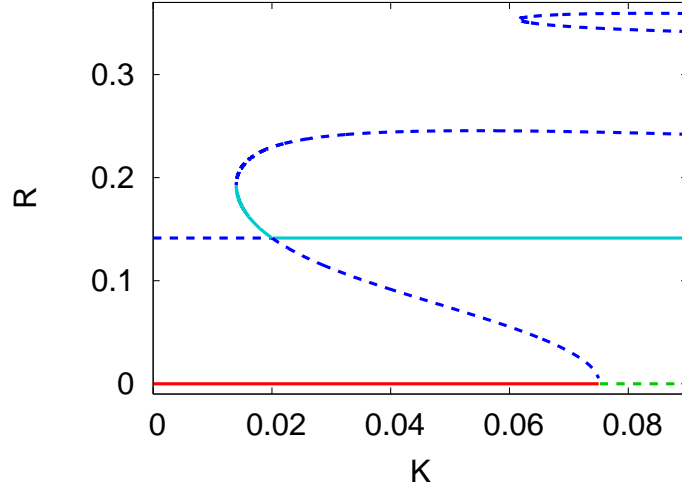


FIG. 7: (Color online) Dependence of the radius  $R$  of the periodic orbits upon the control amplitude  $K$  for  $\gamma = -10$ ,  $\beta = \pi/4$ ,  $\lambda = -0.02$ , and  $\tau$  according to Eq. (3), i.e., along the Pyragas curve. Solid cyan/light : stable limit cycle, dashed blue/dark: unstable periodic orbit, solid red/dark: stable trivial fixed point, dashed green/light: unstable trivial fixed point. Exchange of stability at the transcritical bifurcation and the subcritical Hopf bifurcation are clearly visible (cf. Fig. 6).

to show that the widely accepted odd number limitation theorem [12], which states that periodic orbits with an odd number of positive Floquet exponents cannot be stabilised by time-delayed feedback control, is incorrect. As it was demonstrated [13], the unstable periodic orbit which emerges from a subcritical Hopf bifurcation and which has a single positive Floquet exponent, can indeed be stabilised by time-delayed feedback control if the control force is coupled with a nondiagonal control matrix, parametrised, e.g., by a phase  $\beta$ . The proof of the odd number limitation theorem fails because of the occurrence of a transcritical bifurcation, involving an exchange of stability with other, delay-induced periodic orbits which have previously been overlooked. Technically, the proof of the odd number limitation theorem in [12] fails for autonomous systems because the trivial Floquet multiplier (Goldstone mode) was neglected there[38]. At the transcritical bifurcation, besides the Goldstone mode of the Pyragas orbit, a second Floquet exponent becomes zero. Hence, there exists a Floquet exponent  $\Lambda = 0$  of algebraic multiplicity two but geometric multiplicity one.

For the subcritical Hopf normal form studied here, the Floquet mode problem can be solved analytically because the delay-differential equation linearised around the periodic

orbit gives rise to an autonomous linear system. Thus, the eigenvalues of the Jacobian matrix coincide with the Floquet exponents. In this way the problem becomes tractable on the same footing as time-delayed feedback control of steady states, where full analytical solutions are available [21, 22]. We have derived analytical expressions for the control thresholds and for the bifurcation manifolds including the analysis of delay-induced periodic orbits. Thus, the present analysis opens the possibility to study the influence of delay mismatch on time-delayed feedback control beyond the perturbative regime [23]. This is in contrast, for instance, to the Rössler system, where only a numerical bifurcation analysis of time-delayed feedback control has been performed [24]. Even global features like basins of attraction become accessible for our normal form model, beyond what is already known from direct bifurcation analysis [20]. Since the Hopf bifurcations of limit cycles can be dealt with in an analytical way, the model offers promising perspectives from the point of view of numerical continuation tools, as well [25–28]. Torus solutions which are notoriously difficult to analyse are here accessible for a time delay system although mode locking structures would not show up in our model because of the rotational symmetry of the system.

We have not discussed in full detail the eigenvalue spectra that determine the stability of the Pyragas orbit (cf. appendix B for some examples). For the much simpler case of diagonal control in periodically driven systems the spectra can be expressed in analytical terms by the Lambert W-function [29, 30]. The more sophisticated characteristic equation (14) may be viewed as the natural extension of such an approach and it would be promising to study the full analytical structure of its solutions.

From the point of view of applications it is useful to determine the shape of the control domain in the  $(K, \beta)$  control parameter plane. Actually, using a reduced Cartesian representation,  $\kappa_x = K\tau \cos(\beta)$  and  $\kappa_y = K\tau \sin(\beta)$  (cf. Eq. (4)), Eq. (17) yields the simple expression

$$\kappa_x + \gamma\kappa_y = -1 \tag{20}$$

for the control boundary caused by the transcritical bifurcation. Eq. (14) determines the control boundary caused by the Hopf instability when imaginary eigenvalues are considered. Although no simple expression is obtained for general parameter values, analytical results can be found in the limiting case  $|\lambda| \ll 1$  [13]. Neglecting the second contribution to Eq. (14)



we obtain the parametric representation

$$i\phi + (\kappa_x + i\kappa_y)(1 - \exp(-i\phi)) = 0 \quad (21)$$

where  $i\phi$  denotes the normalised critical eigenvalue. Thus, the asymptotic boundary caused by the Hopf bifurcation does not depend on the period parameter  $\gamma$ . The corresponding asymptotic control domains are displayed in Fig. 8 for different values of  $\gamma$ . It has been pointed out already in [13] that the phase  $\beta$  plays a crucial role since control cannot be achieved with vanishing phase, i.e.  $\kappa_y = 0$ . Furthermore a large value of  $|\gamma|$ , i.e. a substantial dispersion is important as well since otherwise the control domain shrinks considerably. It is tempting to extend these results to finite values of  $\lambda$  and to derive sufficient conditions for successful control in terms of  $K$ ,  $\beta$  and the Floquet exponent of the unstable orbit.

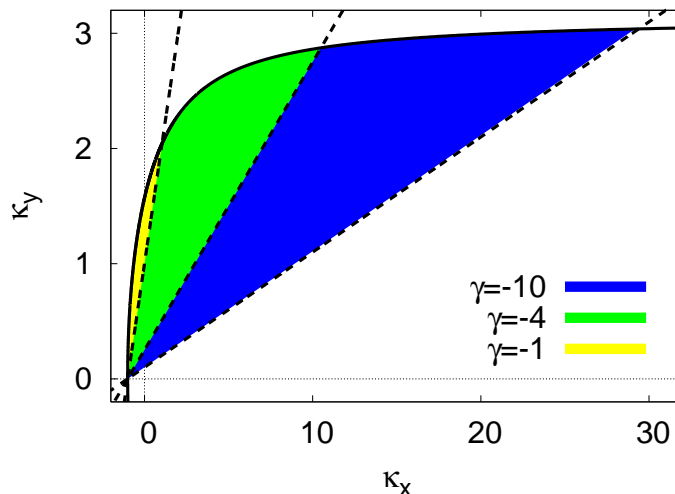


FIG. 8: (Color online) Asymptotic control domain in reduced Cartesian control amplitudes  $\kappa_x = K\tau \cos(\beta)$ ,  $\kappa_y = K\tau \sin(\beta)$  for different values of  $\gamma$ , in the limit  $|\lambda| \ll 1$ . Solid line: upper boundary caused by Hopf instability (cf. Eq. (21)), dashed lines: lower boundary caused by transcritical instability for different values of  $\gamma$  (cf. Eq. (20)). The different control domains overlap.

From the point of view of applications, our result - that stabilisation of unstable periodic orbits generated by a subcritical Hopf bifurcation is possible - looks very promising. For instance, subcritical Hopf bifurcations have been found in laser experiments, recently [31, 32], and the all-optical realisation of time-delayed feedback control via an external Fabry-Perot resonator has been demonstrated [33]. Moreover, the feedback phase of the control signal

which we have found to play a crucial role in the stabilisation arises naturally in laser experiments.

### Acknowledgments

This work was supported by DFG in the framework of Sfb 555.

### APPENDIX A: NORMAL FORM ANALYSIS

The equation of motion (4) can be cast into the general form

$$\dot{\underline{x}}(t) = \underline{\underline{A}} \underline{x}(t) + \underline{\underline{B}} \underline{x}(t - \tau) + C : \underline{x}(t) : \underline{x}(t) : \underline{x}(t) : \quad (\text{A1})$$

where  $\underline{x} = (x_1, x_2)$  abbreviates the state vector, the matrices of the linear part are given by

$$\underline{\underline{A}} = \begin{pmatrix} \lambda - K \cos \beta & -1 + K \sin \beta \\ 1 - K \sin \beta & \lambda - K \cos \beta \end{pmatrix}, \quad \underline{\underline{B}} = K \begin{pmatrix} \cos \beta & -\sin \beta \\ \sin \beta & \cos \beta \end{pmatrix}, \quad (\text{A2})$$

and the nonlinearity is determined by the trilinear expression

$$C : \underline{u} : \underline{v} : \underline{w} := \frac{1}{3} \left( (u_1 v_1 + u_2 v_2) \begin{pmatrix} 1 & -\gamma \\ \gamma & 1 \end{pmatrix} \begin{pmatrix} w_1 \\ w_2 \end{pmatrix} + \text{cycl.} \right) \quad (\text{A3})$$

where the two remaining terms of the sum are obtained by cyclic permutation of the arguments  $u, v, w$ . If we consider parameter values on the Hopf bifurcation line, i.e., Eqs. (7), then the equation of motion can be reduced to the normal form

$$\dot{\zeta}(t) = i\Omega_H \zeta(t) + c |\zeta(t)|^2 \zeta(t) \quad (\text{A4})$$

with complex  $\zeta(t)$  and  $c$ . The sign of  $\text{Re}(c)$  determines whether the bifurcation is super- or subcritical.

Closed analytical expressions for the coefficient  $c$  can be found in the literature (cf. e.g. [8, 34, 35]). The corresponding formula can be easily derived from Eq. (A1) as well since no quadratic nonlinearities are contained in the original equation of motion. To keep our presentation self-contained we just recall the essential steps. Thereby, we follow the approach outlined in [30] which allows for an elementary treatment of differential-difference equations.

The equations for the critical eigenvectors are given by

$$i\Omega_H \underline{u}_c = (\underline{A} + \exp(-i\Omega_H \tau) \underline{B}) \underline{u}_c \quad (\text{A5a})$$

$$i\Omega_H \underline{v}_c^* = \underline{v}_c^* (\underline{A} + \exp(-i\Omega_H \tau) \underline{B}) \quad . \quad (\text{A5b})$$

If  $\underline{x}_t(\theta) = \underline{x}(t + \theta)$  denotes the state of the delay system where the variable  $-\tau \leq \theta \leq 0$  takes the history of the dynamics into account, then the expansion of the centre manifold of the delay system reads

$$\underline{x}(t + \theta) = \underline{x}_t(\theta) = \zeta(t) \exp(i\Omega_H \theta) \underline{u}_c + \zeta^*(t) \exp(-i\Omega_H \theta) \underline{u}_c^* + \text{h.o.t.} \quad . \quad (\text{A6})$$

The higher-order terms can be chosen to be at least of third order in the small amplitude  $\zeta$ . If we introduce eigenfunctions and their dual through

$$\underline{U}_c(\theta) = \exp(i\Omega_H \theta) \underline{u}_c \quad (\text{A7a})$$

$$\underline{V}_c^*(\theta) = \underline{v}_c^* (\delta(\theta + 0) + \underline{B} \exp(-i\Omega_H(\theta + \tau))), \quad (\text{A7b})$$

where  $\delta$  denotes the  $\delta$ -distribution, and define the inner product to be

$$\langle \underline{V}_c | \underline{U}_c \rangle = \int_{-\tau}^0 \underline{V}_c^*(\theta) \underline{U}_c(\theta) d\theta \quad (\text{A8})$$

then orthogonality of the eigenfunctions and Eq. (A6) yield

$$\zeta(t) \langle \underline{V}_c | \underline{U}_c \rangle = \langle \underline{V}_c | \underline{x}_t \rangle = \underline{v}_c^* \underline{x}(t) + \int_{t-\tau}^t \exp(-i\Omega_H(\theta + \tau - t)) \underline{v}_c^* \underline{B} \underline{x}(\theta) d\theta \quad (\text{A9})$$

if the higher-order contributions of the centre manifold are normalised to be orthogonal to the linear eigenspace. Taking the time derivative of Eq. (A9), using the equation of motion (A1), the eigenvalue condition (A5), and the definition (A9), we get

$$\dot{\zeta}(t) \langle \underline{V}_c | \underline{U}_c \rangle = i\Omega_H \zeta(t) \langle \underline{V}_c | \underline{U}_c \rangle + \underline{v}_c^* C : \underline{x}(t) : \underline{x}(t) : \underline{x}(t) : \quad . \quad (\text{A10})$$

If we now insert for the phase space coordinate  $\underline{x}(t)$  the expression given by the centre manifold, Eq. (A6) with  $\theta = 0$ , and discard the non resonant cubic contributions which can be eliminated by an additional coordinate transformation then the cubic coefficient of the normal form (A4) can be found as

$$c = \frac{3\underline{v}_c^* C : \underline{u}_c : \underline{u}_c : \underline{u}_c^* :}{\langle \underline{V}_c | \underline{U}_c \rangle} = \frac{3\underline{v}_c^* C : \underline{u}_c : \underline{u}_c : \underline{u}_c^* :}{\underline{v}_c^* \underline{u}_c + \underline{v}_c^* \underline{B} \underline{u}_c \exp(-i\Omega_H \tau) \tau} \quad . \quad (\text{A11})$$

Calculation of the eigenvectors is quite straightforward with Eqs. (A5), when using the expressions (A2) and the characteristic equation (cf. Eq. (6)). We obtain

$$\underline{u}_c = \begin{pmatrix} 1 \\ -i \end{pmatrix}, \quad \underline{v}_c^* = (1, i) \quad . \quad (\text{A12})$$

Taking the definition (A3) into account, the cubic coefficient evaluates as

$$c = \frac{4(1 + i\gamma)}{1 + K\tau \exp(i\beta - i\phi)} \quad . \quad (\text{A13})$$

Thus, apart from the complex valued normalisation in the denominator the cubic coefficient coincides with the cubic coefficient of the original equation of motion (1). But the denominator turns out to be crucial. The condition on the sign of the real part, determining the type of Hopf bifurcation, results in Eq. (8).

## APPENDIX B: CHARACTERISTIC EQUATION FOR PERIODIC SOLUTIONS

Let us consider a general system where the linear part has a vanishing and a positive eigenvalue,  $\mu > 0$ , so that the corresponding matrix in a diagonal basis reads

$$\underline{\underline{A}} = \begin{pmatrix} 0 & 0 \\ 0 & \mu \end{pmatrix} \quad . \quad (\text{B1})$$

If  $\underline{\underline{B}}$  denotes the control matrix the stability properties of time-delayed feedback control are determined by the characteristic equation

$$\begin{aligned} 0 &= \det(z - \underline{\underline{A}} + \underline{\underline{B}}(1 - \exp(-z))) \\ &= z(z - \mu) + z(1 - \exp(-z))\text{tr}(\underline{\underline{B}}) - (1 - \exp(-z))\mu B_{11} + (1 - \exp(-z))^2 \det(\underline{\underline{B}}) \end{aligned} \quad (\text{B2})$$

If we choose

$$\mu = -2\lambda\tau > 0 \quad (\text{B3a})$$

$$\text{tr}(\underline{\underline{B}}) = 2K\tau \cos \beta \quad (\text{B3b})$$

$$B_{11} = K\tau(\cos \beta + \gamma \sin \beta) \quad (\text{B3c})$$

$$\det(\underline{\underline{B}}) = (K\tau)^2 \geq 0 \quad (\text{B3d})$$

then the expression (B2) indeed coincides with the characteristic equation (14) governing the stability of the Pyragas orbit. But it is to some extent simpler to analyse the general

expression (B2). Of course, Eq. (B2) admits the trivial solution  $z = 0$  which corresponds to the Goldstone mode. We constrain the three control parameters  $\text{tr}(\underline{\underline{B}})$ ,  $\det(\underline{\underline{B}})$ , and  $B_{11}$  to two independent variables by introducing the condition

$$B_{11} = \sigma \text{tr}(\underline{\underline{B}}) \quad (\text{B4})$$

with some fixed parameter  $\sigma$ . Then the solutions of Eq. (B2) can be analysed in a two-dimensional parameter plane.

In a first step we concentrate on small real valued solutions of Eq. (B2). A Taylor series expansion along the lines of section IV yields

$$z = \frac{\mu\sigma}{1 - 1/\sigma - \mu/2 + \det(\underline{\underline{B}})} (\text{tr}(\underline{\underline{B}}) + 1/\sigma) + \mathcal{O}((\text{tr}(\underline{\underline{B}}) + 1/\sigma)^2) \quad . \quad (\text{B5})$$

Thus, a real solution triggers a change of stability at

$$\text{tr}(\underline{\underline{B}}) = -1/\sigma \quad (\text{B6})$$

and the coefficient in Eq. (B5) decides on which side of the bifurcation line the mode is stable or unstable, respectively.

To determine a parametric representation of the Hopf bifurcation line, use  $z = i\phi$  and split Eq. (B2) into real and imaginary part

$$0 = -\phi^2 - \text{tr}(\underline{\underline{B}})\phi \sin \phi - \mu\sigma \text{tr}(\underline{\underline{B}})(1 - \cos \phi) - 2\det(\underline{\underline{B}})(1 - \cos \phi) \cos \phi \quad (\text{B7a})$$

$$0 = -\mu\phi + \text{tr}(\underline{\underline{B}})\phi(1 - \cos \phi) - \mu\sigma \text{tr}(\underline{\underline{B}}) \sin \phi + 2\det(\underline{\underline{B}})(1 - \cos \phi) \sin \phi \quad . \quad (\text{B7b})$$

Taking linear combinations of both equations with  $\sin \phi$  and  $\cos \phi$  the independent variables can be decoupled and we end up with

$$\text{tr}(\underline{\underline{B}}) = -\frac{\phi^2 \sin \phi + \mu\phi \cos \phi}{\phi(1 - \cos \phi) + \mu\sigma \sin \phi} \quad (\text{B8a})$$

$$\det(\underline{\underline{B}}) = \frac{-\phi^2 \cos \phi + \mu\phi \sin \phi - (\phi \sin \phi - \mu\sigma(1 - \cos \phi)) \text{tr}(\underline{\underline{B}})}{2(1 - \cos \phi)} \quad . \quad (\text{B8b})$$

In addition, by implicit differentiation of Eq. (B2) one can easily derive a criterion on which side of the bifurcation line (B8) the complex conjugated pair yields a stable or unstable eigenmode, respectively.

Both bifurcation lines, Eqs. (B6) and (B8), can be displayed easily in the  $\text{tr}(\underline{\underline{B}})$ - $\det(\underline{\underline{B}})$  parameter plane. The yet undetermined parameter  $\sigma$  can be identified from Eqs. (B3b), (B3c), and (B4) to be

$$\sigma = (1 + \gamma \tan \beta)/2 \quad . \quad (\text{B9})$$

Furthermore, the control scheme implemented in Eq. (1) yields the conditions (B3b) and (B3d), i.e., the constraint

$$\det(\underline{\underline{B}}) = (\text{tr}(\underline{\underline{B}})/(2 \cos \beta))^2 \quad . \quad (\text{B10})$$

Thus, the particular control scheme traces a path along a parabola where the parameter  $\text{tr}(\underline{\underline{B}})$  is proportional to the control amplitude. Results for  $\gamma = -10$ ,  $\beta = \pi/4$ , and  $\lambda = -0.02$  are displayed in Fig. 9. On increasing the control amplitude a transcritical bifurcation takes place and an interval of successful control is entered. Its upper bound is caused by a Hopf bifurcation. In fact, the control path only explores a tiny region of the full control domain.

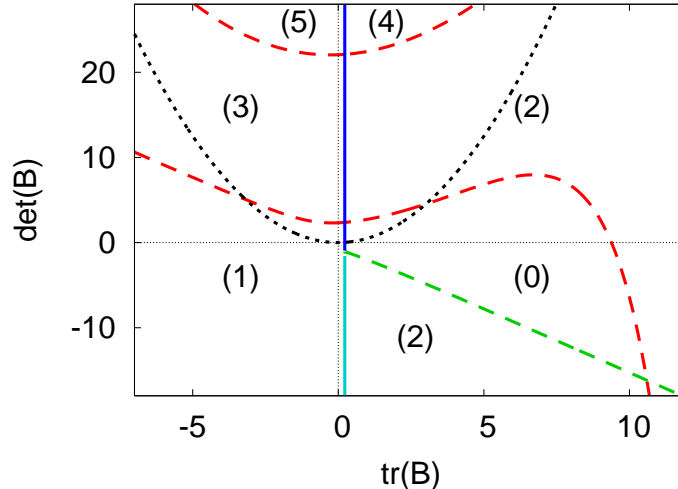


FIG. 9: (Color online) Bifurcation diagram of the characteristic equation (B2) in a two-dimensional parameter plane for  $\gamma = -10$ ,  $\beta = \pi/4$ , and  $\lambda = -0.02$ . Solid blue/cyan: transcritical bifurcation, Eq. (B6) (unstable eigenvalue occurs left/right of the line). Dashed red/green: Hopf bifurcation, Eq. (B8) (unstable eigenvalues occur above/below the line). Dotted black: bifurcation path traced by the control scheme, cf. Eq. (B10). Labels indicate the number of unstable eigenvalues.

If one decreases  $\lambda$ , i.e., if one considers unstable orbits with larger Lyapunov exponent the control domain shrinks considerably in size and finally may even disappear completely. Beyond a certain critical value for  $\lambda$  which, in our case can be computed from Eqs. (B8) and (B10) to be  $-\lambda\tau = \mu/2 = 1 - 1/\sigma + 1/(2\sigma \cos \beta)^2$ , the control path misses the control domain and stabilisation is not possible any more (cf. Fig. 10). Thus the control scheme shows features known from control of orbits with complex Floquet exponents [19].

The same features are of course visible as well if one computes numerically the correspond-

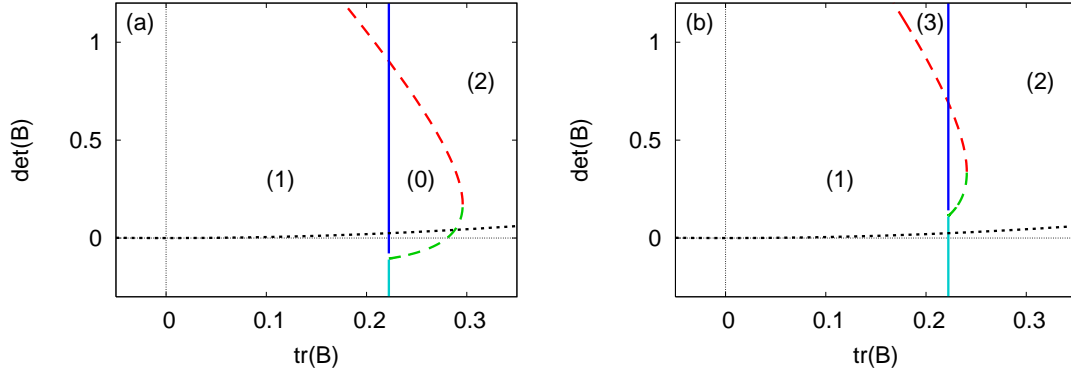


FIG. 10: (Color online) Bifurcation diagrams for the characteristic equation (B2) in a two-dimensional parameter plane for  $\gamma = -10$ ,  $\beta = \pi/4$  and different values of  $\lambda$ : (a)  $\lambda = -0.064$ , (b)  $\lambda = -0.068$ . Solid blue/cyan: transcritical bifurcation, Eq. (B6) (unstable eigenvalue occurs left/right of the line). Dashed red/green: Hopf bifurcation, Eq. (B8) (unstable eigenvalues occur above/below the line). Dotted black: bifurcation path traced by the control scheme, cf. Eq. (B10). Labels indicate the number of unstable eigenvalues.

ing Floquet spectra, e.g. the solutions of the characteristic equation (14) in dependence on the control amplitude. Figure 11 shows such data for the parameter settings used in Fig. 10. Clearly, a finite but small control interval is visible which is going to disappear when the parameter  $\lambda$  increases in modulus.

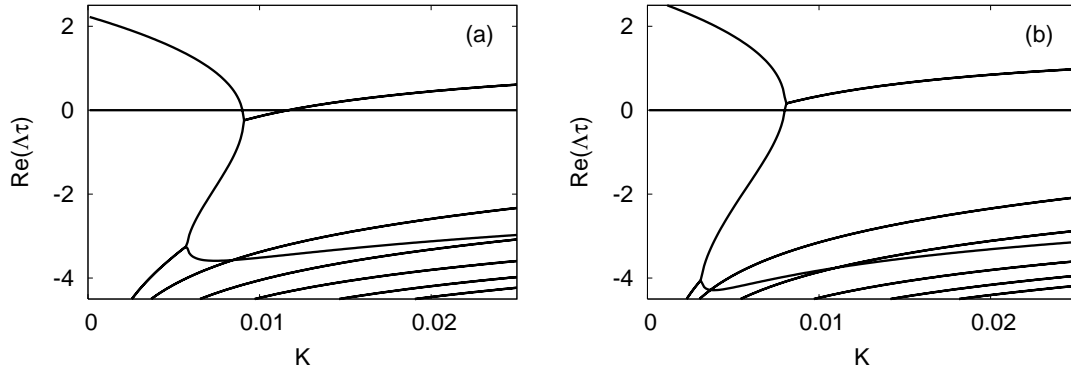


FIG. 11: Floquet spectrum (real part of the exponents) in dependence on the control amplitude for  $\gamma = -10$ ,  $\beta = \pi/4$  and two different values of  $\lambda$ : (a)  $\lambda = -0.064$ , (b)  $\lambda = -0.068$  (cf. Fig. 10).

## APPENDIX C: CENTRE MANIFOLDS, $S^1$ -SYMMETRY, AND STABILITY OF ROTATING WAVES

In this appendix we conceptually summarise – from a mathematical perspective – the above calculations on Pyragas stabilisation of the Hopf model (1). Specifically, we address  $S^1$ -equivariance and co-rotating coordinates  $z(t) = e^{i\omega t}\zeta(t)$ , rotating waves and their bifurcations, the role of centre manifolds, and bifurcation to non-rotating waves.

For any fixed real  $\omega$ , the transformation  $z(t) = e^{i\omega t}\zeta(t)$  to co-rotating complex coordinates  $\zeta(t)$  transforms Eq. (1) into the equivalent delay equation

$$\dot{\zeta}(t) = (\lambda + (1 - \omega)i)\zeta(t) + (1 + i\gamma)|\zeta(t)|^2\zeta(t) - K \exp(i\beta) (\zeta(t) - e^{-i\omega\tau}\zeta(t - \tau)) \quad . \quad (\text{C1})$$

The co-rotating equation (C1) is autonomous since  $e^{i\theta}z(t)$  solves Eq. (1) for any fixed real  $\theta$ , whenever  $z(t)$  does. Steady states  $\dot{\zeta} = 0$  of Eq. (C1) are precisely the rotating waves of Eq. (1), i.e., solutions of the form  $z(t) = e^{i\omega t}\zeta_0$  with nonzero rotation frequency  $\omega$  and nonzero  $\zeta_0 \in \mathbb{C}$ . The minimal period of such solutions  $z(t)$  is of course given by  $T = 2\pi/|\omega|$ . The Pyragas curves are determined by  $\tau = mT = 2\pi m/|\omega|$  for positive integers  $m = 1, 2, 3, \dots$

Rotating waves are nontrivial steady states  $\zeta(t) = \zeta_0$  of Eq. (C1), i.e., solutions of

$$0 = \lambda + (1 - \omega)i + (1 + i\gamma)|\zeta_0|^2 - K \exp(i\beta) (1 - e^{-i\omega\tau}) \quad . \quad (\text{C2})$$

All bifurcation diagrams above are concerned with solutions  $(\omega, |\zeta_0|^2)$  of Eq. (C2) only. We can solve this equation for real parts (cf. Eq. (18a))

$$|\zeta_0|^2 = -\lambda - K[\cos(\beta - \omega\tau) - \cos(\beta)] \quad (\text{C3})$$

under the constraint of a positive right hand side. Substituting into the imaginary part of Eq. (C2) yields the real equation (cf. Eq. (18b))

$$1 - \omega + K[\sin(\beta - \omega\tau) - \sin(\beta)] - \gamma\{\lambda + K[\cos(\beta - \omega\tau) - \cos(\beta)]\} = 0 \quad . \quad (\text{C4})$$

We seek solutions  $\omega$ , depending on the five real parameters  $\lambda, \gamma, K, \beta, \tau$ . The degenerate case  $\omega = 0$  which corresponds to a circle of equilibria, alias a frozen wave of vanishing angular velocity  $\omega$ , arises only for  $\gamma\lambda = 1$  [36].

Note how the fold description, in two parameters  $(\lambda, \tau)$ , of the transcritical bifurcation along the Pyragas curve  $\tau = 2\pi/|\omega|$  follows from Eq. (C4) when we plot  $\omega$  (or  $|\zeta_0|^2$ ) as a



function of  $(\lambda, \tau)$ , for fixed suitable  $\gamma, K, \beta$  (cf. Figs. 1 and 5). Indeed, all this follows if we explicitly solve Eq. (C4) for  $\lambda$ , as a function of  $\gamma, K, \beta, \tau, \omega$ , and then project the resulting graph onto whatever parameter plane we desire.

At the Hopf bifurcation we have a simple pair of purely imaginary eigenvalues, and no other imaginary eigenvalues. Therefore, the centre manifold is two-dimensional at the Hopf bifurcation [9]. Dimension two also holds at the transcritical bifurcation of rotating waves. Moreover, the centre manifold can be chosen to be invariant with respect to the  $S^1$  action  $z \mapsto e^{i\theta}z$  [37]. In polar coordinates the dynamics in any two-dimensional centre manifold is therefore given by a system of the general form

$$\dot{r} = f(r^2, \underline{\mu})r \quad (\text{C5a})$$

$$\dot{\varphi} = g(r^2, \underline{\mu}) \quad (\text{C5b})$$

with parameter vector  $\underline{\mu}$ , i.e., in our case  $\underline{\mu} = (\lambda, \gamma, K, \beta, \tau)$ . Note that  $\varphi$  does not enter the equation for  $\dot{r}$  or  $\dot{\varphi}$ . Indeed,  $(r, \varphi + \theta)$  must be a solution for any fixed  $\theta$ , by  $S^1$ -equivariance, whenever  $(r, \varphi)$  is. Also note that Eq. (C5) is a system of differential equations which does not involve time delayed arguments. Rather, the original time delay  $\tau$  enters as one parameter among others.

To determine  $f$  we observe that  $f(r^2, \underline{\mu}) = 0$  defines rotating (or frozen) waves with  $|\zeta_0| = r$ , and thus must be equivalent to Eq. (C2) with  $g(r^2, \underline{\mu}) = \omega$ . The solution set  $(r^2, \omega, \underline{\mu})$  is therefore given by Eqs. (C3) and (C4) again, and defines the zero set of  $f$ . Again,  $f(r^2, \underline{\mu}) = 0$  if, and only if,  $(\omega, \underline{\mu})$  solve Eq. (C4) and  $r^2$  is given by Eq. (C3).

To determine the stability of our rotating waves within the centre manifold it remains to determine the sign of  $f$  outside the zero set. That sign is known at the trivial equilibrium  $r = 0$ , by standard exchange of stability at nondegenerate Hopf bifurcations. Normally hyperbolic rotating waves correspond to simple zeros of  $f$  in the  $r$ -direction, i.e.,  $\partial_r g \neq 0$ . This allows us to determine the sign of  $g$ , and then of  $f$ , in all bifurcation diagrams. The (in-)stability properties of all rotating waves within the two-dimensional centre manifold follows. By spectral analysis at the Hopf bifurcation (or at the transcritical bifurcation of rotating waves) (in-)stability in the full delay system (1) follows from the centre manifold analysis without ever computing the manifold itself.

Rotating waves  $z(t) = e^{i\omega t}\zeta_0$  are periodic solutions of Eq. (1). But not all periodic solutions need to be rotating waves. Any bifurcation from rotating waves, however, must

be visible in co-rotating coordinates  $\zeta(t) = e^{-i\omega t} z(t)$  as well. Since rotating waves of Eq. (1) are equilibria of Eq. (C1) any such bifurcation must be accompanied by purely imaginary eigenvalues  $\Lambda$  of the characteristic equation associated to  $\zeta_0$ . Not only along the Pyragas curve this characteristic equation was derived in Eq. (14).

It may be useful to insert  $\Lambda = i\omega$  here and check for the resulting curve for  $K, \beta$  such that Eq. (14) holds. Such a curve would discover torus bifurcations from rotating waves or, equivalently, Hopf bifurcations from (circles of) nontrivial equilibria  $\zeta_0$  of Eq. (C1). Due to  $S^1$ -equivariance such tori would exhibit neither phase-locking nor devil's staircases, but smooth dependence of rotation numbers on parameters.

- 
- [1] K. Pyragas, Phys. Lett. A **170**, 421 (1992).
  - [2] *Handbook of Chaos Control*, edited by E. Schöll and H. G. Schuster (Wiley-VCH, Weinheim, 2007), second completely revised and enlarged edition.
  - [3] J. E. S. Socolar, D. W. Sukow, and D. J. Gauthier, Phys. Rev. E **50**, 3245 (1994).
  - [4] N. Baba, A. Amann, E. Schöll, and W. Just, Phys. Rev. Lett. **89**, 074101 (2002).
  - [5] O. Beck, A. Amann, E. Schöll, J. E. S. Socolar, and W. Just, Phys. Rev. E **66**, 016213 (2002).
  - [6] J. Unkelbach, A. Amann, W. Just, and E. Schöll, Phys. Rev. E **68**, 026204 (2003).
  - [7] J. Schlesner, A. Amann, N. B. Janson, W. Just, and E. Schöll, Phys. Rev. E **68**, 066208 (2003).
  - [8] J. K. Hale and S. M. Verduyn Lunel, *Introduction to Functional Differential Equations* (Springer, New York, 1993).
  - [9] O. Diekmann, S. A. van Gils, S. M. Verduyn Lunel, and H. O. Walther, *Delay Equations* (Springer-Verlag, New York, 1995).
  - [10] M. E. Bleich and J. E. S. Socolar, Phys. Lett. A **210**, 87 (1996).
  - [11] W. Just, T. Bernard, M. Ostheimer, E. Reibold, and H. Benner, Phys. Rev. Lett. **78**, 203 (1997).
  - [12] H. Nakajima, Phys. Lett. A **232**, 207 (1997).
  - [13] B. Fiedler, V. Flunkert, M. Georgi, P. Hövel, and E. Schöll, Phys. Rev. Lett. **98**, 114101 (2007).
  - [14] B. van der Pol, Phil. Mag. **7**(2), 978 (1926).

- [15] R. Lang and K. Kobayashi, IEEE J. Quantum Electron. **16**, 347 (1980).
- [16] M. C. Cross and P. C. Hohenberg, Rev. Mod. Phys. **65**, 851 (1993).
- [17] Y. Kuramoto, Prog. Theor. Phys. Suppl. **79**, 223 (1984).
- [18] J. Guckenheimer and P. Holmes, *Nonlinear Oscillations, Dynamical Systems, and Bifurcations of Vector Fields* (Springer-Verlag, New York, 1986).
- [19] W. Just, E. Reibold, H. Benner, K. Kacperski, P. Fronczak, and J. Holyst, Phys. Lett. A **254**, 158 (1999).
- [20] W. Just, H. Benner, and C. v. Löwenich, Physica D **199**, 33 (2004).
- [21] P. Hövel and E. Schöll, Phys. Rev. E **72**, 046203 (2005).
- [22] S. Yanchuk, M. Wolfrum, P. Hövel, and E. Schöll, Phys. Rev. E **74**, 026201 (2006).
- [23] W. Just, D. Reckwerth, J. Möckel, E. Reibold, and H. Benner, Phys. Rev. Lett. **81**, 562 (1998).
- [24] A. G. Balanov, N. B. Janson, and E. Schöll, Phys. Rev. E **71**, 016222 (2005).
- [25] K. Engelborghs, T. Luzyanina, and D. Roose, J. Comp. Appl. Math. **125**, 265 (2000).
- [26] K. Engelborghs, T. Luzyanina, and G. Samaey, Technical Report No. TW-330, Department of Computer Science, K.U.Leuven, Belgium (unpublished).
- [27] K. Engelborghs, T. Luzyanina, and D. Roose, ACM Transactions on Mathematical Software **28**, 1 (2002).
- [28] J. Hizanidis, R. Aust, and E. Schöll, Int. J. Bifur. Chaos (2007), in print.
- [29] R. M. Corless, G. H. Gonnet, D. E. G. Hare, D. J. Jeffrey, and D. E. Knuth, Adv. Comput. Math **5**, 329 (1996).
- [30] A. Amann, E. Schöll, and W. Just, Physica A **373**, 191 (2007).
- [31] S. Bauer, O. Brox, J. Kreissl, B. Sartorius, M. Radziunas, J. Sieber, H. J. Wünsche, and F. Henneberger, Phys. Rev. E **69**, 016206 (2004).
- [32] O. V. Ushakov, H. J. Wünsche, F. Henneberger, I. A. Khovanov, L. Schimansky-Geier, and M. A. Zaks, Phys. Rev. Lett. **95**, 123903 (2005).
- [33] S. Schikora, P. Hövel, H. J. Wünsche, E. Schöll, and F. Henneberger, Phys. Rev. Lett. **97**, 213902 (2006).
- [34] F. Giannakopoulou and A. Zapp, Physica D **159**, 215 (2001).
- [35] B. F. Redmond, V. G. LeBlanc, and A. Longtin, Physica D **166**, 131 (2002).
- [36] B. Fiedler, *Global bifurcation of periodic solutions with symmetry*, Vol. 1309 of *Lect. Notes*

*Math.* (Springer-Verlag, Heidelberg, 1988).

[37] A. Vanderbauwhede, *Dynamics Reported* **2**, 89 (1989).

[38]  $F(1) = G(1) = 0$  in equation (14) in [12] and not less than zero, as assumed (A. Amann, priv. comm.).